(Received 24 November 2025, Accepted 5 January 2026, Scheduled 1 February 2026)

A Compact Comb Shaped Wearable Antenna for Biomedical Applications

Prathipati Rakesh Kumar[1, *], Challa Rama Krishna[2], Kavuri Vijayachandra[3], Pamarthi Sunitha[4], and Chaitanya K. Marpu[5]

[1]*Department of ECE, Lakireddy Bali Reddy College of Engineering, Mylavaram, India*
[2]*Vignan Institute of Technology and Science, Deshmukhi, Telangana, India*
[3]*PACE Institute of Technology, Ongole, Andhra Pradesh, India*
[4]*Department of ECE, Aditya University, Surampalem, Andhra Pradesh, India*
[5]*Department of ECE, Aditya Institute of Technology and Management, Tekkali, Andhra Pradesh, India*

ABSTRACT: A comb-shaped antenna was designed, optimized, and analyzed for an operational frequency of 2.4 GHz. The proposed design was modelled on an RT/Duroid 2880 substrate with dimensions $32 \times 28\,mm^2$ and 0.8 substrate thickness. The antenna is designed to resonate at 2.4 GHz frequency band on substrate material. The body placement analysis of the proposed antenna was performed using human hand and leg phantom models, and the Specific Absorption Ratio (SAR) was less than 1.6 w/kg (ranging 0–0.361 W/kg on hand and 0–0.267 W/kg on leg phantoms, respectively). The 3D radiation gains for both the hand and leg are 4.95 and 4.81, respectively. Additionally, the vertical and horizontal bending losses were taken at 0°, 30°, 45°, 60° degrees, respectively, and their graphs were analyzed. Owing to its efficient and effective results, this antenna can be utilized for various biomedical applications.

1. INTRODUCTION

In the age of omnipresent connectivity, wearables have become crucial elements in healthcare, fitness, and communication networks. Antenna is central to wearables, tasked with flawless wireless transmission of data. The antenna design for wearables presents challenges specific to the wearables' location close to the human body, impacting performance via the detuning and absorption of radiation. Rigid antenna designs are lacking in terms of flexibility, comfort, and biocompatibility. This paper presents the design and analysis of a comb-shaped microstrip patch antenna at 2.4 GHz. The antenna is constructed on RT/Duroid Rogers 2880, which is a low-loss and flexible substrate. The new structure is intended to provide higher gain, radiation efficiency, and safety while maintaining a Specific Absorption Ratio (SAR) within acceptable limits. Its small size and conformal structure make it a good candidate for body-worn applications. The simulation results showed enhanced impedance matching and radiation stability. The work contributes to the increasing demand for efficient and reliable wearable antenna solutions in communication systems.

A comprehensive overview of flexible wearable antennas explores various aspects such as design constraints, materials, fabrication techniques, and their roles in WBANs and healthcare monitoring are explored, with a focus on maintaining performance under deformation and environmental stress [1]. An ultra-wideband (UWB) antenna is integrated with a metamaterial for wearable applications [2], where SAR analysis ensures compliance with safety standards. Similarly, the design challenges and potential solutions for biomedical flexible antennas have also been addressed [3]. A miniaturized hexagonal dual-band antenna is optimized for on-body operation, while using human body phantoms and SAR simulations for evaluating wearable suitability [4, 5].

Several studies have focused on antenna performance in proximity to the human body. For instance, [6] offers a review of various wearable antenna designs for both on-body and off-body communications, highlighting trade-offs in size, shape, gain, and SAR. SAR evaluations specific to healthcare-focused UWB antennas are carried out, employing hexagonal and fractal geometries, respectively, [7, 8]. Reviews of miniaturized, flexible antennas incorporating SAR considerations for body area networks (BANs) have been reported in [9, 10], with the latter also proposing a novel FSS-based reflector to reduce SAR. Medical-oriented wearable antennas have been reported in [11], where SAR is simulated on a realistic arm phantom [12], where an FSS absorber is employed for SAR mitigation in millimeter-wave applications.

Novel compact wearable antenna structures utilize hybrid quasi-fractal designs [13, 14], both emphasizing SAR and bending performance over the human body. Research proposes UWB wearable antennas with reduced SAR for radiative near-field wireless power transfer and durable multi-slotted configurations, reporting SAR levels under FCC limits. Body effect mitigation via flexible periodic structures and innovative AMC/SIW cavity-backed designs [15–18] enhance radiation performance and safety. The performance of low-SAR flexible antennas in the ISM band has been investigated in [9], while the suitability of wearable antennas through phantom-based testing

* Corresponding author: Prathipati Rakesh Kumar (rakeshkumar1774@gmail.com).

is discussed in [20]. Finally, body absorption, frequency shifts, and efficiency losses in slot antennas [21–26] emphasize the impact of biological tissues on 2.4–2.45 GHz wearable devices through computational simulations. The manuscript is organized as follows. Section 2 describes the antenna design. Section 3 presents the simulated results of the parametric analysis of antenna bending losses, both vertical and horizontal, along with SAR analysis. Section 4 presents measured results. Finally, Section 5 includes the key findings and possible improvements in the future work as the conclusion.

2. PROPOSED ANTENNA DESIGN

The development of wearable technology created a growing need for flexible, small, and high-performance antennas. Among the many designs, patch antenna has been highlighted because of its low profile, simplicity of integration with textile substrates, and attractive radiation characteristics. Nonetheless, in wearable use, impedance matching and radiation performance need to be optimized as a result of body proximity effects and movement caused distortion. This study focused on the design and optimization of a wearable patch antenna through the insertion of a comb-like structure within the radiating patch. This is done to increase impedance matching without compromising the radiation features of the antenna. The improved patch structure is presented in Fig. 1(a), and dimensions are shown in Table 1, wherein several geometrical parameters are primarily responsible for determining the performance of the antenna.

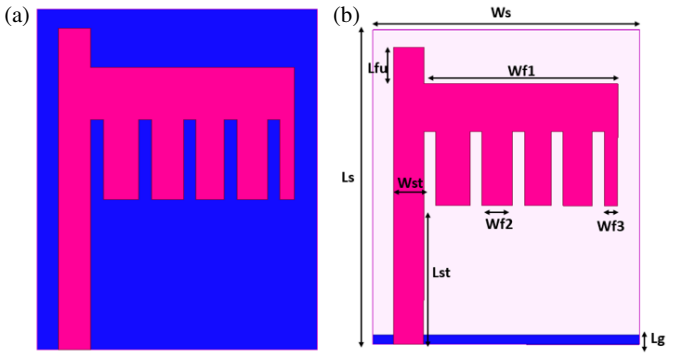

FIGURE 1. (a) Antenna without DGS. (b) With DGS.

Calculation of the patch width:

$$width = \frac{c}{2f_0\sqrt{\frac{\varepsilon_r+1}{2}}} \tag{1}$$

where c is the light velocity, f_0 the operating frequency, and ε_r the relative permitivity.

Effective dielectric constant:

$$(\varepsilon_{eff}) = \frac{\varepsilon_r+1}{2} + \frac{\varepsilon_r-1}{2}\left[\frac{1}{\sqrt{1+12\left(\frac{h}{w}\right)}}\right] \tag{2}$$

h is the height of the substrate.

TABLE 1. Antenna parameters and their respective values.

Name of the parameter	Symbol	Value (mm)
Length of the ground	L_g	2
Length of the substrate	L_s	34
Width of the substrate	W_s	22
Length of the strip	L_{st}	15
Width of the strip	W_{st}	2.5
Width of the single comb	W_{f2}	2.8
Width of a space in comb	W_{f3}	1
Width of the patch flag	W_{f1}	18.5
Length of patch upper rectangle	L_{fu}	2

Calculation of the patch length:

$$length = \frac{c}{2f_0\sqrt{\varepsilon_{eff}}} - 0.824h\left(\frac{\varepsilon_r\left(\varepsilon_{eff}+0.3\right)\left(\frac{w}{h}+0.264\right)}{\left(\varepsilon_{eff}-0.258\right)\left(\frac{w}{h}+0.8\right)}\right) \tag{3}$$

The guided wavelength and quality parameters of the designed antenna are optimised for improved radiation efficiency. Antennas can achieve low values of reflection coefficients in the desired frequency band ($S_{11} < -10$ dB) with perfect matching. The gain (G) and directivity (D) of the proposed antenna correlate with radiation efficiency. Gain (G) is usually expressed in decibels (dB) and given as G (dB) $= 10 \times \log_{10}(\eta_{\text{rad}} D)$.

3. RESULTS AND DISCUSSIONS

3.0.1. Using Various Iterations

The antenna design was realized through various iterative steps with step-by-step improvements aimed at improving the performance for biomedical purposes. The basic rectangular monopole from iteration 1 is shown in Fig. 2(a), which had limited bandwidth and single-band operation, and the design was first improved by incorporating multiple vertical slots in the second iteration as shown in Fig. 2(b). This significantly improved the return loss and moved the resonance closer to the 3.8 GHz ISM band. In the last structure in Fig. 2(c), the slot geometry was further optimized in terms of length, width, and spacing, which led to better impedance matching and wider bandwidth. The S_{11} plot in Fig. 3 clearly shows

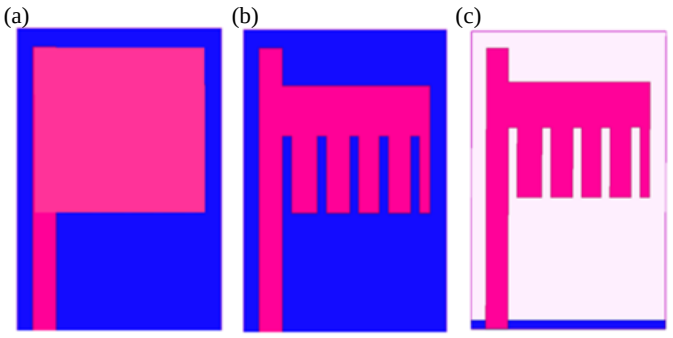

FIGURE 2. (a) Iteration 1. (b) Iteration 2. (c) Iteration 3.

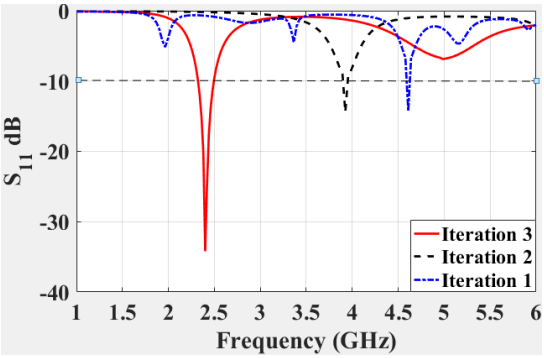

FIGURE 3. S_{11} parameter plot comparing all iterations.

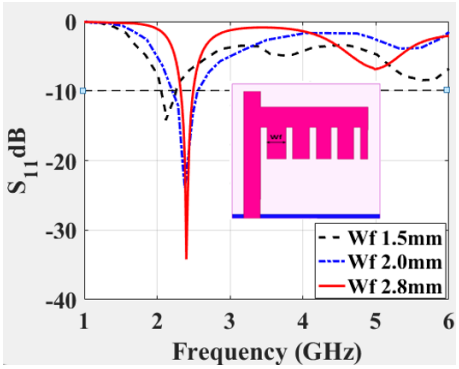

FIGURE 4. S_{11} parameter comparison for different slot widths.

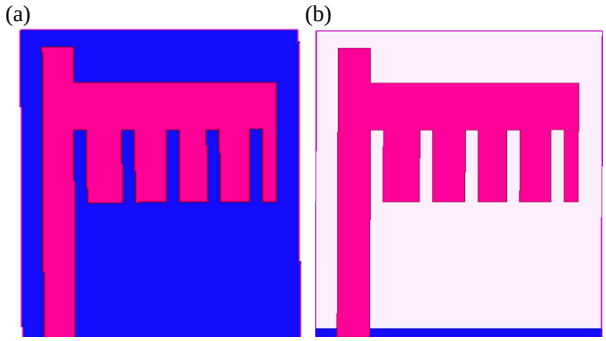

FIGURE 5. Proposed antenna. (a) Without DGS. (b) With DGS.

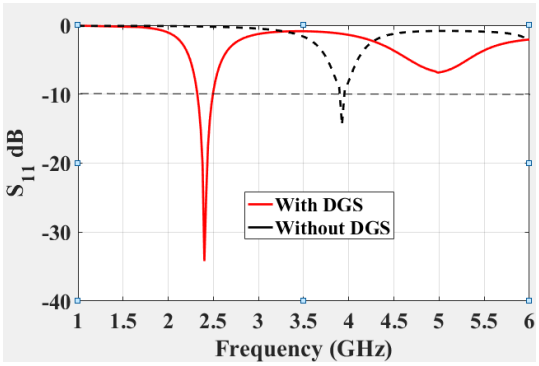

FIGURE 6. Simulated return loss of designed antenna without and with DGS.

the improvement, where the final structure (black curve) exhibits single-band performance and deep resonance at around 2.4 GHz, which is suitable for body-centric wireless communication. The final antenna has a compact size, flexibility, and low SAR and is thus highly suitable for wearable biomedical devices operating over UWB and ISM frequencies.

3.0.2. Return Loss Variation with Different Flag Widths

The design of the antenna was also improved by altering the width of the slots within the radiating patch. The alterations entail a gradual widening of the flag-shaped slots towards increasing the bandwidth and impedance matching. The 2.5 mm width strip displays the initial design with equal slot widths. The flag widths were moderately increased from 1.5 mm to 2.8 mm to study their impact on antenna performance. The resulting S_{11} parameter values, shown in Fig. 4, exhibit significant enhancement in the return loss with altered widths.

3.0.3. Return Loss Curves with and without Defected Ground Structure

To improve the performance of the antenna, a defected ground structure (DGS) was added, as shown in Figs. 5(a) and 5(b). The antenna without the DGS can be seen in Fig. 5(a), and Fig. 5(b) illustrates the improved structure with the addition of the DGS to the ground plane. Its introduction aims to reduce surface wave propagation, improve impedance matching, and achieve a broader bandwidth. The S_{11} comparison shown in Fig. 6 demonstrates conclusively that the antenna with DGS shows greatly enhanced return loss behaviour, especially near the dual-band resonant frequencies. The improved performance is apparent from the deeper and sharper resonances below the -10 dB line, indicating better impedance matching and higher radiation efficiency. Therefore, the inclusion of DGS was an extremely useful modification in achieving optimized performance for wearable applications.

3.0.4. Variability in Return Loss for Various DGS

The effects of different DGSs on the performance of the antenna are illustrated using Fig. 7(a) to Fig. 7(c), and Fig. 7(a) represents the comb-shaped baseline antenna with original DGS and is used as the reference. For the purpose of studying improvement methods, three DGS geometries — dumbbell in Fig. 7(c),

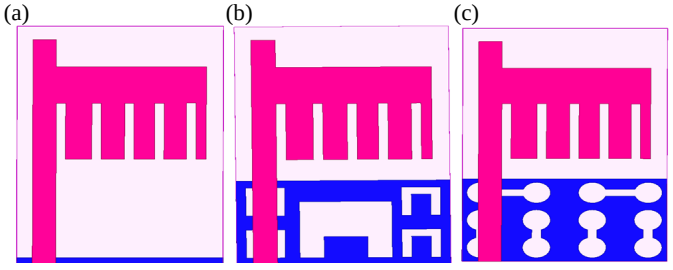

FIGURE 7. (a) Original DGS. (b) Reverse-U shaped DGS. (c) Dumbbell shaped DGS.

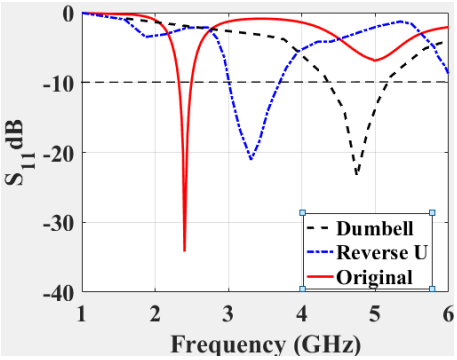

FIGURE 8. Simulated return loss curves for different DGSs.

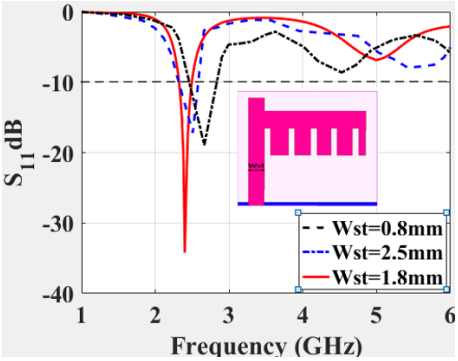

FIGURE 9. Simulated return loss curves for different strip widths (W_{st}).

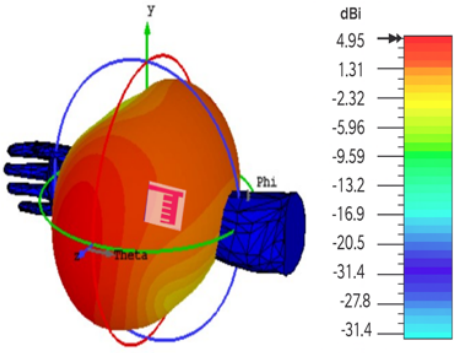

FIGURE 10. Hand phantom radiation pattern with gain plot.

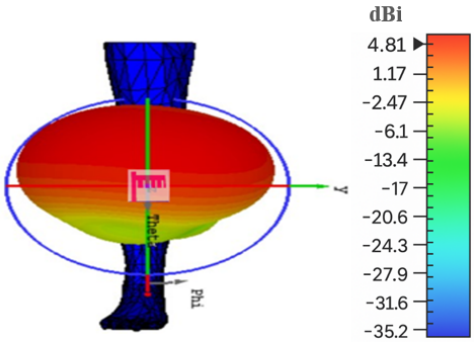

FIGURE 11. Leg phantom radiation pattern with gain plot.

reverse-U in Fig. 7(b), and the proposed DGS (Original) in Fig. 7(a) — were added into the ground plane. The respective reflection coefficient responses (S_{11}) show significant improvements. The comb-shaped (original) DGS saw the greatest improvement, with a sharp and deep resonance at 2.4 GHz and an S_{11} of less than -30 dB as shown in Fig. 8, which reflects very good impedance matching. The dumbbell DGS provides a dual-resonance characteristic with better bandwidth but comparatively moderate return loss, whereas the reverse-U DGS demonstrates superior performance to the dumbbell but is still inferior to the comb-shaped configuration. This comparison clearly shows the comb-shaped DGS as the best option for achieving maximum antenna efficiency as well as return loss performance.

3.0.5. Variability in Return Loss for Various Strip Feed Widths W_{st}

Different feedline strip widths (W_{st}) of the antenna configuration are 2.5, 1.8, and 0.8, respectively. Fig. 9 displays the corresponding return loss (S_{11}) behavior for each scenario. With the increase in strip width from narrowest W_{st} to widest W_{st}, there is a clear shift in resonance frequency and S_{11} curve depth. The 0.8 mm strip width (W_{st}) antenna has the optimum performance, with a deep resonance at around 3.3 GHz and an S_{11} of less than -20 dB, showing good impedance matching. The 2.5 mm strip width (W_{st}) design has a lower resonance depth, whereas the 1.8 mm (W_{st}) model has two resonances but lower return loss depth. These findings validate that the feedline strip width has a strong influence on the impedance characteristics and tuning of the resonant frequency of the antenna, thereby supporting antenna optimization.

3.1. Radiation Performance Analysis and Their Gain Plots

In this section, the radiation performance of the designed comb-shaped wearable antenna is analyzed under different conditions. The analysis is structured into two parts: hand phantom analysis and leg phantom analysis, each of which provides detailed information along with related images to depict the radiation characteristics and gain performance.

3.1.1. Hand Phantom Analysis

When an antenna is brought close to a hand phantom, its radiation properties are affected by the dielectric nature of the hand. The radiation pattern in this setup illustrates the effect of the hand on beam shape and energy distribution. In Fig. 10, the radiation pattern of the antenna is shown, featuring the main lobe as well as any side lobes owing to the close proximity of the hand. The gain performance indicates that the measured gain is nearly 4.95 dBi, which shows that, despite the hand loading effect, the antenna has strong performance that is appropriate for wearable use.

3.1.2. Leg Phantom Analysis

A comparable test was performed with a leg phantom to determine the antenna's performance in the vicinity of the lower extremities. The radiation pattern obtained in this setup, as shown

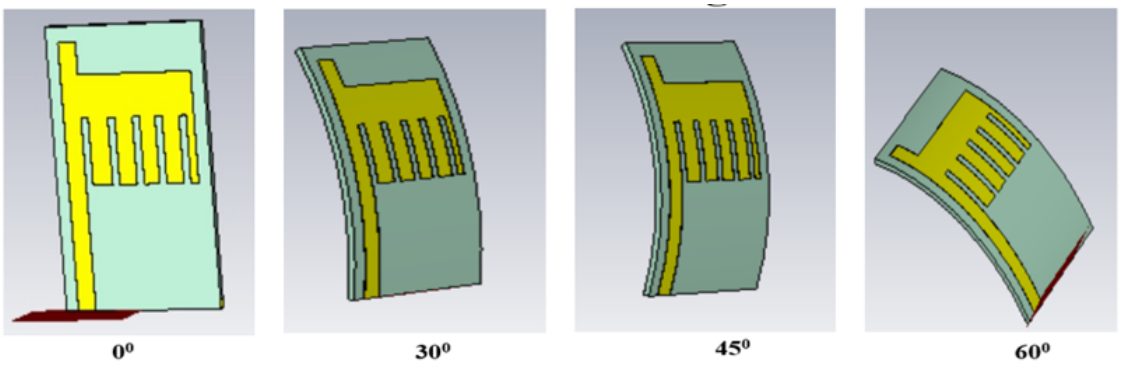

FIGURE 12. Antenna performance at a 0°, 30°, 45°, 60° vertical bend, respectively.

in Fig. 11, illustrates the impact of the leg's dielectric properties on the direction and strength of the beam. The corresponding gain plot shows a slightly lower gain of approximately 4.81 dBi. The difference is due to the varying geometrical and dielectric properties of the leg as opposed to the hand. Overall, the leg phantom analysis verifies that the antenna works accurately, even under on-body conditions for various parts of the body.

3.2. Bending Losses

In wearable antenna applications, bending the antenna along various axes can significantly influence its impedance matching and radiation characteristics. In this work, bending losses in two principal orientations, vertical and horizontal, are discussed. For both, separate images for various bending percentages are provided along with a combined graph to demonstrate the overall effect. Bending introduces structural deformation, resulting in a frequency shift and the possible detuning of the antenna. When the bending radius was reduced, the return loss increased, signifying an increased reflection of the signal. Such degradation may impair communication quality in body-centric communications.

3.2.1. Vertical Bending Losses

Vertical bending is the deformation in the direction of the antenna height that produces variations in the current distribution and effective electrical length. This section describes the vertical bending loss encountered at various bending angles as shown in Fig. 12 and return loss plot as shown in Fig. 13. Wearable devices experience bending or deformation in various directions during typical use. To ensure consistent and reliable communication, it is essential to understand how vertical bending affects the antenna's functionality. The proper consideration of these effects is critical for maintaining optimal performance and efficiency in wearable applications.

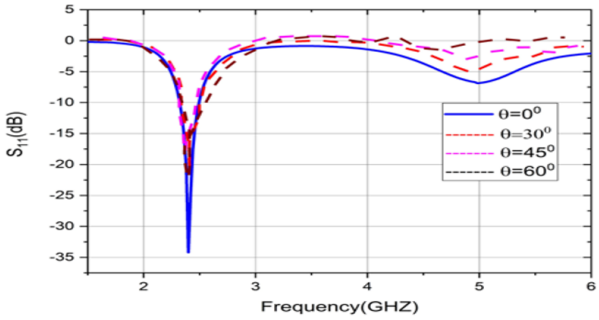

FIGURE 13. Return loss plot at 0°, 30°, 45°, 60° vertical bend, respectively.

The graph illustrates how the return loss and radiation efficiency change as the bending angle is increased. The analysis shows that with a higher bending angle, the impedance mismatch increases, causing greater bending losses and a frequency shift in the resonance.

3.2.2. Horizontal Bending Losses

Horizontal bending is the bending along the width of the antenna, which influences the current distribution and radiation pattern differently from vertical bending. Fig. 14 and Fig. 15 show the horizontal bending loss. An analysis of the horizontal bending data shows that at vertical bending, the baseline performance is optimal at 0°. Increasing the bending angle enhanced the horizontal bending losses, which are due to the distortion of the current distribution in the width direction. The combined graph assists in the identification of crucial bending limits, above which the performance of the antenna is drastically degraded, prompting for design methods for countering these effects in realistic wearable application.

The combined overview illustrates the overall effect on return loss and radiation patterns. It is evident that horizontal bending also leads to performance deterioration, but the type of loss and frequency shifts may be different from vertical bending because of the distinct physical deformation.

3.3. Specific Absorption Rate (SAR) Analysis

SAR is an essential parameter for checking the safety of wearable antennas, especially when they situate in close proximity to the human body. SAR measures the rate at which biological tissues absorb electromagnetic energy when they are exposed to radio frequency (RF) fields. In the present study, SAR calculations were performed with both hand and leg phantoms to estimate the levels of radiation absorption and to ensure compliance of the antenna with international exposure guidelines.

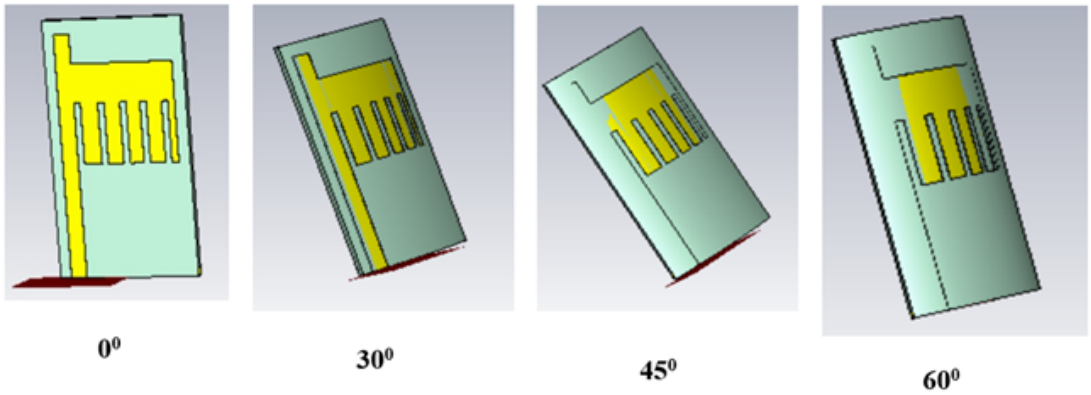

FIGURE 14. Antenna performance at 0°, 30°, 45°, 60° horizontal bend.

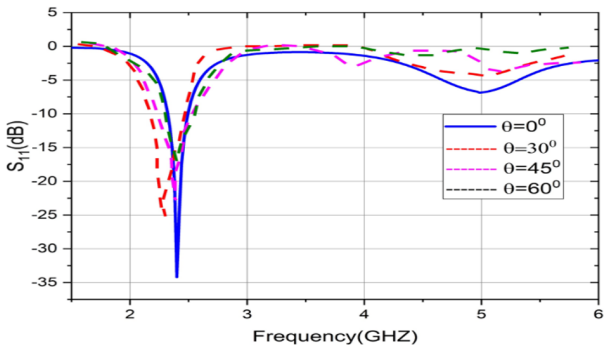

FIGURE 15. Return loss plot at 0°, 30°, 45°, 60° horizontal bend respectively.

3.3.1. Hand Phantom SAR Analysis

In the hand phantom setup, the proposed comb-shaped antenna was mounted on a realistic human arm model to assess the amount of RF energy absorbed by the tissues. The SAR distribution obtained using this setup is shown in Fig. 16(a), which shows the colour-mapped intensity of absorption across the forearm. The highest SAR value recorded in this configuration was 0.361 W/kg, as indicated by the colour scale in Fig. 16(b). This value is significantly below the regulatory threshold of 1.6 W/kg for localized exposure (averaged over 1 g of tissue), confirming the safety of the design. The simulation demonstrates a localized but safe distribution of energy, concentrated primarily near the antenna placement area.

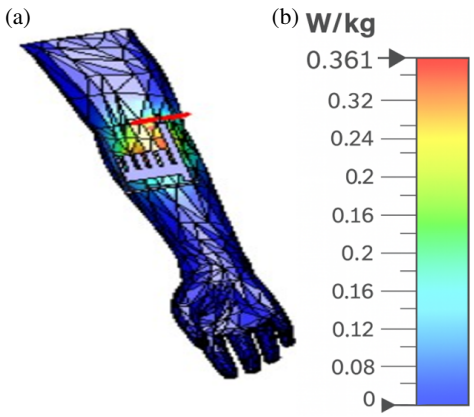

FIGURE 16. (a) Hand phantom. (b) Hand phantom SAR values.

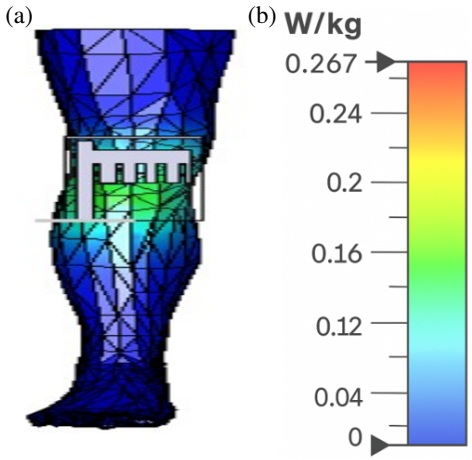

FIGURE 17. (a) Leg phantom. (b) Leg phantom SAR values.

3.3.2. Leg Phantom SAR Analysis

The SAR measurement was also conducted with a human leg phantom to determine the interaction of the antenna with lower-body anatomical tissues, including skin, subcutaneous fat, and muscle. As indicated in Fig. 17(a), the SAR distribution indicates a wider spread of energy absorption owing to the larger surface area of contact. The maximum SAR value here is also found to be 0.267 W/kg, as indicated on the scale bar in Fig. 17(b). This value remains below the 1.6 W/kg regulatory limit for 1 g averaged tissue, confirming design safety. The simulation validates that the antenna has robust SAR performance across all positions and may be placed on various parts of the body, which ensures that it is applicable for various wearable purpose.

3.4. Field Distribution Analysis

To examine the electromagnetic performance of the designed comb-shaped wearable antenna, the electric field (E-field), magnetic field (H-field), and surface current distribution were studied using full-wave simulations at the resonant frequency of 2.4 GHz. These field distributions are essential in determining radiation behavior, impedance characteristics, and the effectiveness of the antenna within wearable environments. The E-field distributions, as shown in Fig. 18, indicate the highest electric field intensities in the vicinity of the feedline and the

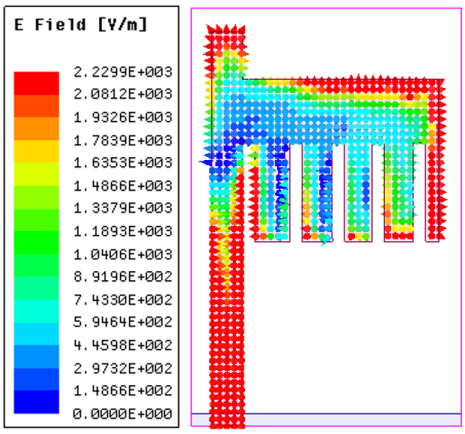

FIGURE 18. Distribution of electric field (E-field) of the designed antenna at 2.4 GHz.

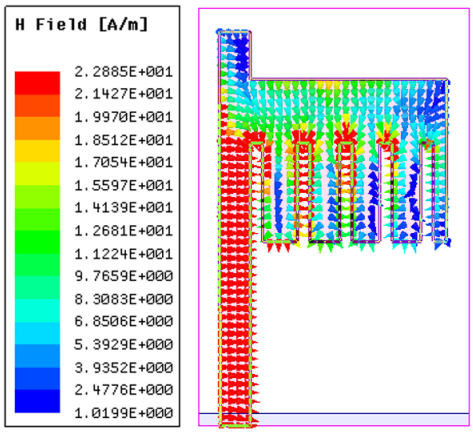

FIGURE 19. Magnetic field (H-field) distribution of the designed antenna at 2.4 GHz.

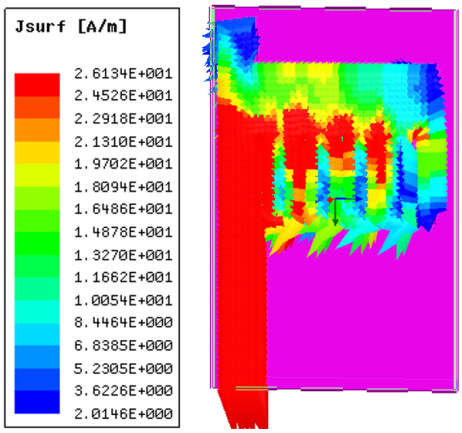

FIGURE 20. Surface current density (Jsurf) distribution of the proposed antenna at 2.4 GHz.

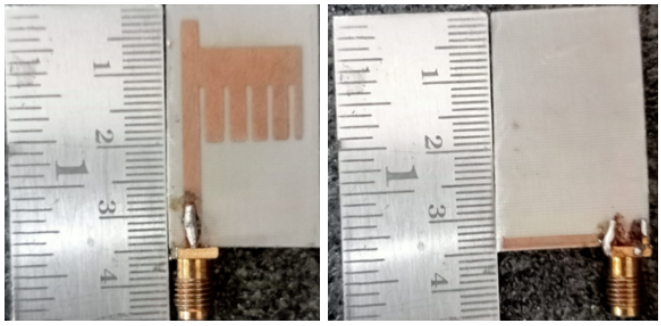

FIGURE 21. Fabricated antenna top view and bottom view.

edges of the comb slot. This reflects efficient radiation and high reactive field behavior within the active region of the antenna.

The H-field patterns in Fig. 19 show well-distributed magnetic field loops, particularly around the vertical parts of the comb structure, which are the magnetic equivalent of the radiated energy, providing correct antenna resonance and impedance matching.

Lastly, the surface current density plots in Fig. 20 indicate that the highest surface currents are situated close to the feed and outer arms of the comb-like structure. This behavior validates the optimal current flow and efficient excitation of radiating elements.

4. MEASURED RESULTS AND DISCUSSIONS

The prototype of the proposed comb-shaped microstrip antenna, which was fabricated as shown in Fig. 21, was tested to demonstrate its simulated behaviour. The antenna was fabricated on an RT/Duroid 2880 substrate of 0.8 mm thickness with the help of high-precision etching and connected through SMA connectors. A Vector Network Analyzer (VNA) and an anechoic chamber were employed to measure the return loss, gain, and radiation patterns.

4.1. Measured and Simulated Return Loss

The simulated and measured return loss responses of the proposed antenna are shown in Fig. 22. A significant correlation is evident between them, thereby validating the desired resonance frequency at 2.4 GHz. The slight frequency deviation observed in the measured data can be ascribed to the fabrication toler-

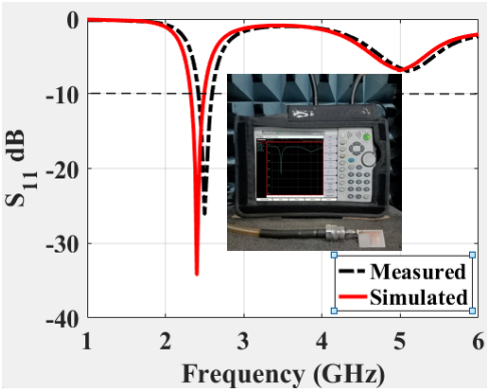

FIGURE 22. Measured and simulated return losses for proposed antenna.

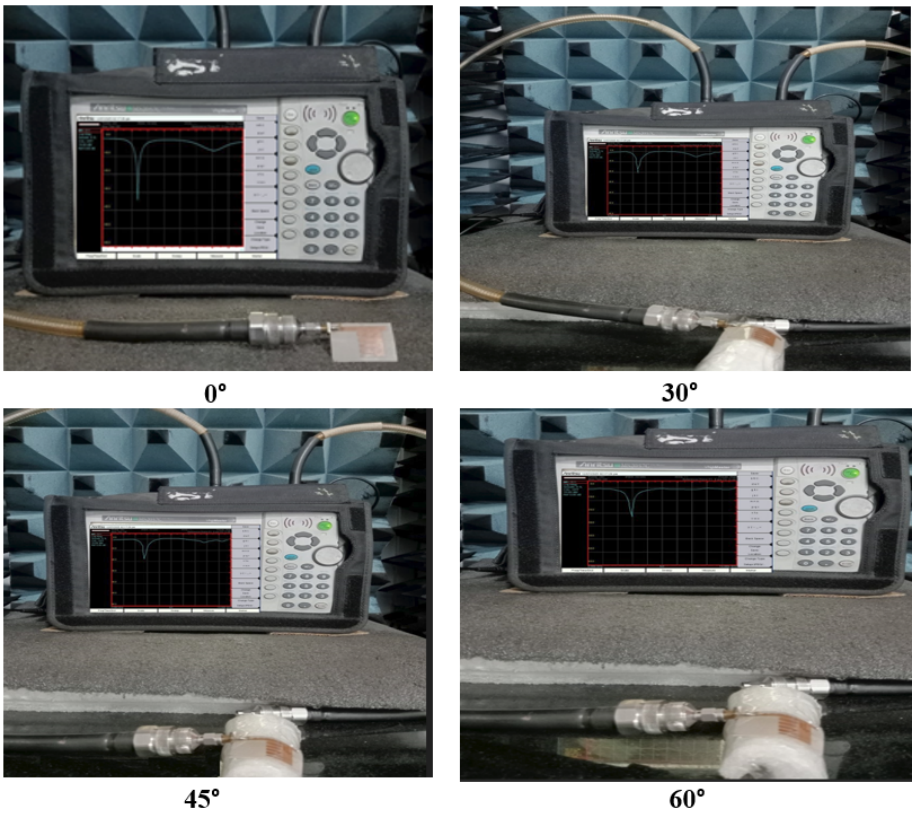

FIGURE 23. Vertical bending measurement setup of the proposed antenna at 0°, 30°, 45°, and 60°.

ances and soldering effects in proximity to the feed region. In summary, the empirical response substantiates the durability of the proposed design and its appropriateness for 2.4 GHz wearable applications. An Anritsu MS2037C series Vector Network Analyzer is used for measuring the reflection coefficient (S_{11}) of the fabricated prototype antenna.

The prototype was further evaluated under practical deformation conditions by bending the antenna vertically at 0°, 30°, 45°, and 60°, as depicted in Fig. 23. The measured return loss responses for each bending angle, shown in Fig. 24, demonstrate the antenna's ability to sustain an acceptable impedance performance under bending, which is essential for wearable applications.

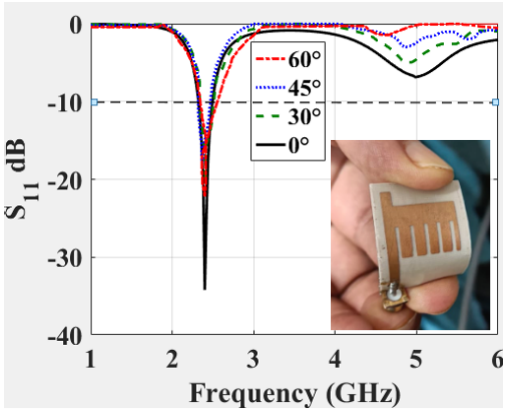

FIGURE 24. Measured return loss plot at 0°, 30°, 45°, 60° vertical bend.

Furthermore, horizontal bending analysis was performed by bending the fabricated antenna at angles of 0°, 30°, 45°, and 60° while maintaining proper VNA connectivity, as illustrated in Fig. 25. The measured return loss responses shown in Fig. 26 indicate that the antenna retains satisfactory impedance matching performance under horizontal bending, demonstrating its suitability for conformal and body-mounted applications.

4.2. Voltage Wave Standing Wave Ratio (VSWR)

The designed antenna exhibits a VSWR of less than 1.5 as shown in Fig. 27 which includes the simulated and measured results.

4.3. Polar Plot Analysis

To ascertain the far-field radiation patterns, the fabricated antenna was evaluated within an anechoic chamber. The far-field radiation characteristics of the proposed antenna exhibited a bidirectional pattern, which was derived from measurements conducted in the anechoic chamber and is illustrated in Fig. 28. The measured and simulated plots of the E and H fields for the proposed antenna are taken at a frequency of 2.4 GHz, shown in Fig. 29. The analysis of the radiation patterns in the E-plane and H-plane illustrated agreement with simulations, displaying a directional nature and conformity in performance.

The superior comparison and presentation of our proposed antenna are systematically compiled through pertinent previously reported research in Table 2. The designed antenna has a compact size and maintains SAR values well below the safety

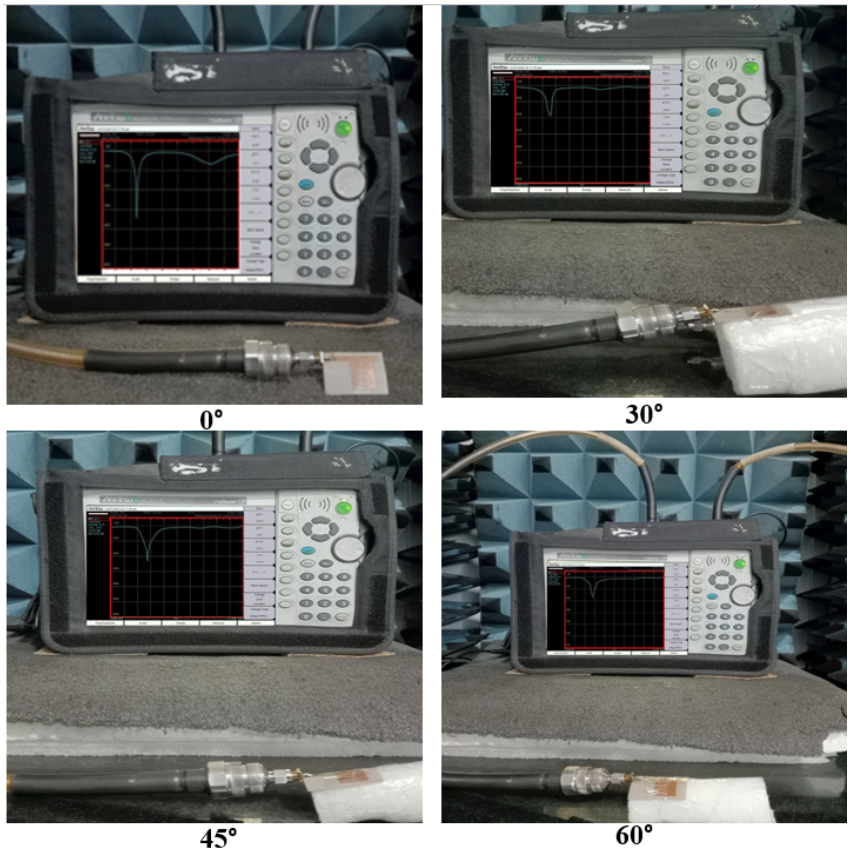

FIGURE 25. Horizontal bending measurement setup of the proposed antenna at 0°, 30°, 45°, and 60°.

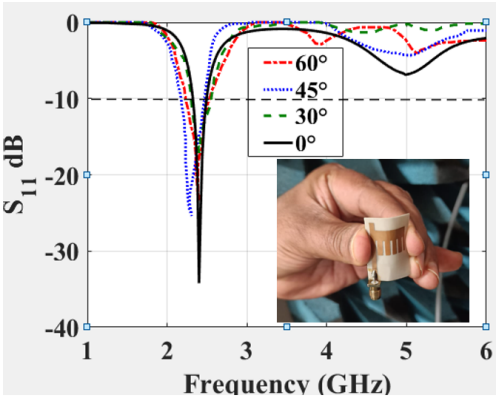

FIGURE 26. Measured return loss plot at 0°, 30°, 45°, 60° horizontal bend.

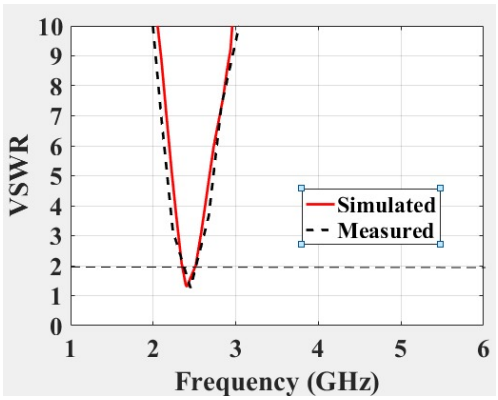

FIGURE 27. VSWR of the proposed antenna.

TABLE 2. Comparison of the recommended antenna with existing works

Reference Paper number	Operating Frequency	Dimensions (mm)	Bandwidth (GHz)	SAR (W/kg)	Gain (dBi)
[7]	3.8–5.2 GHz	28 × 24 × 1.6	1.4	0.56(max)	4.6
[13]	2.45 GHz	35 × 25 × 1.0	0.5	0.29(max)	3.2
[15]	2.35 GHz	40 × 30 × 1.6	0.32	1.56(max)	4.1
[14]	3.1–10.6 GHz	38 × 30 × 1.2	7.5	0.94(max)	4.3
[10]	2.45 GHz	42 × 34 × 1.5	0.36	0.74(max)	4.0
Proposed Antenna	2.4 GHz	32 × 28 × 0.8	0.41	0.36(hand), 0.267(leg)	4.95(hand), 4.81(leg)

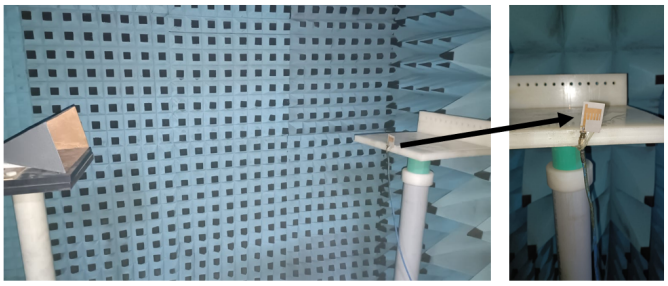

FIGURE 28. Photograph of anechoic chamber setup.

limit while providing sufficient gain for both hand and leg positions. This emphasizes the strength of the antenna in striking a balance among efficiency, safety, and compactness, thus making it highly suitable for wearable biomedical applications.

5. CONCLUSION

In this paper, a comb-shaped antenna designed on an RT/Duroid 2880 substrate with a compact size of $32 \times 28\,\text{mm}^2$ and thickness of 0.8 mm successfully resonates at the 2.4 GHz ISM band, ensuring suitability for wearable communication systems. On-body performance evaluation showed that the SAR values remained well below the permissible limit of 1.6 W/kg, with measured ranges of 0–0.361 W/kg on the human hand phantom and 0–0.267 W/kg on the leg phantom, confirming user safety. The antenna also achieved stable radiation characteristics with peak 3D gain values of 4.95 dBi (hand) and 4.81 dBi (leg). Mechanical robustness was verified through bending tests under vertical and horizontal deformations of 0°, 30°, 45°, and 60° with acceptable performance variations observed. Overall, the antenna exhibits efficient, safe, and flexible operation, making it a promising candidate for wireless health-monitoring systems.

ACKNOWLEDGEMENT

The authors sincerely acknowledge the financial support provided by Lakireddy Bali Reddy College of Engineering (Autonomous), Mylavaram, NTR District, Andhra Pradesh, India, under the Seed Money Project (Project File No. LBRCE/R&D/2023-24/Seed/04).

REFERENCES

[1] Singh, S., R. Mishra, A. Kapoor, and S. Singh, "A comprehensive review and analysis of the design aspects, structure, and applications of flexible wearable antennas," *Telecom*, Vol. 6, No. 1, 3, Jan. 2025.

[2] Douhi, S., Y. Houssaini, S. Das, V. Subramanian, B. T. P. Madhav, M. Mazroui, and A. Eddiai, "Metamaterial-integrated wearable UWB antenna with SAR reduction and gain enhancement for Wireless Body Area Sensor Networks (WBASNs): Design and experimental verification," *Sensors and Actuators A: Physical*, Vol. 388, 116499, 2025.

[3] Giftsy, A. L. S., U. K. Kommuri, and R. P. Dwivedi, "Flexible and wearable antenna for biomedical application: Progress and opportunity," *IEEE Access*, Vol. 12, 90 016–90 040, 2024.

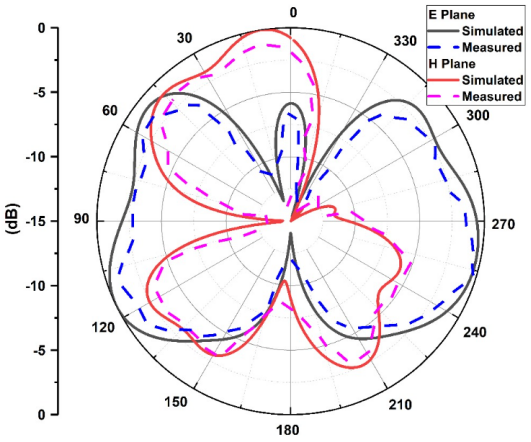

FIGURE 29. Measured and simulated E and H plane radiation patterns at 2.4 GHz.

[4] Burra, A. S. and A. Swamy, "Design and evaluation of a compact unified hexagonal dual-band wearable antenna," *Heliyon*, Vol. 11, No. 5, e02496, 2025.

[5] Ali, U., S. Ullah, J. Khan, M. Shafi, B. Kamal, A. Basir, J. A. Flint, and R. D. Seager, "Design and sar analysis of wearable antenna on various parts of human body, using conventional and artificial ground planes," *Journal of Electrical Engineering and Technology*, Vol. 12, No. 1, 317–328, 2017.

[6] Soni, G. K., D. Yadav, and A. Kumar, "A comprehensive review of wearable antenna design for On-Body and Off-Body communication," *International Journal of Electronics and Telecommunications*, 525–532, 2024.

[7] Karad, K. V., V. S. Hendre, J. L. Rajput, V. Kadam, V. E. Narawade, R. Bakale, and G. D. Londhe, "A SAR analysis of hexagonal-shaped UWB antenna for healthcare applications," *EURASIP Journal on Wireless Communications and Networking*, Vol. 2024, 72, Sep. 2024.

[8] Pathak, P. A., S. L. Nalbalwar, A. E. Wagh, and J. L. Rajput, "A fractal approach to investigate SAR of HMSA UWB antenna for medical applications," *Progress In Electromagnetics Research C*, Vol. 154, 67–75, 2025.

[9] Pandey, U., P. Singh, and R. Singh, "Review on miniaturized flexible wearable antenna with SAR considerations," *Materials Today: Proceedings*, Vol. 66, Part 8, 3667–3674, 2022.

[10] Sharma, S. and M. R. Tripathy, "Wearable antenna with reduced SAR using novel FSS reflector for IoT assisted wireless healthcare applications," *Progress In Electromagnetics Research M*, Vol. 123, 1–11, 2024.

[11] Bangeles, J. M., E. M. Tapawan, and E. Arboleda, "Wearable antennas in medical applications: A comprehensive review of design, performance, safety, and clinical applications," *Preprints*, 2024.

[12] Lee, C., H. Wang, and T. Zhang, "SAR mitigation analysis using millimeter wave antenna with FSS-based absorber for 5G application," *e-Prime — Advances in Electrical Engineering, Electronics and Energy*, Vol. 2, Article 100428, 2024.

[13] Yalduz, H., T. E. Tabaru, V. T. Kilic, and M. Turkmen, "Design and analysis of low profile and low SAR full-textile UWB wearable antenna with metamaterial for WBAN applications," *AEU - International Journal of Electronics and Communications*, Vol. 126, 153465, 2020.

[14] Sapna, B. A., K. Ramasamy, M. G. Krishnan, S. Dhanyasree, and S. Jegadesh, "Design and analysis of a UWB antenna with reduced SAR for early detection of brain tumour," *Antennas for In-*

dustrial and Medical Applications with Optimization Techniques for Wireless Communication, 1st edition, CRC 2024.

[15] Pinapati, S. P., J. Brittain, A. Caldow, and C. Fumeaux, "Wearable textile EBG-inspired bandwidth-enhanced patch antenna," *IET Microwaves, Antennas & Propagation*, Vol. 14, No. 15, 2011–2019, 2020.

[16] Thangavelu, Y., B. Thangaraju, and R. Maheswar, "Design and SAR analysis of an AMC-integrated Wearable cavity-backed SIW antenna," *Micromachines*, Vol. 15, No. 12, 1530, 2024.

[17] Ashyap, A., R. Raad, F. Tubbal, W. A. Khan, and S. Abulgasem, "Comprehensive review of wearable antennas with flexible periodic structures for body-effect mitigation," *IEEE Access*, Vol. 13, 22 590–22 636, 2025.

[18] Giftsy, A. L. S., U. K. Kommuri, and R. P. Dwivedi, "Flexible and wearable antenna for biomedical application: Progress and opportunity," *IEEE Access*, Vol. 12, 90 016–90 040, 2023.

[19] Tiwari, A., A. A. Khurshid, and K. Sharma, "Compact wearable microstrip antenna design using hybrid quasi-Newton and Taguchi optimization," *Scientific Reports*, Vol. 15, No. 1, 116, 2025.

[20] Ali, U., S. Ullah, J. Khan, M. Shafi, B. Kamal, A. Basir, J. Flint, and R. Seager, "Design and sar analysis of wearable antenna on various parts of human body, using conventional and artificial ground planes," *Journal of Electrical Engineering and Technology*, Vol. 12, No. 1, 317–328, 2017.

[21] Karad, K. V. and V. S. Hendre, "A hexagonal shape fractal flexible UWB antenna based on jeans material for healthcare applications," *The Journal of The Textile Institute*, Vol. 116, No. 7, 1227–1242, 2025.

[22] Karad, K. V. and V. S. Hendre, "A flower bud-shaped flexible UWB antenna for healthcare applications," *EURASIP Journal on Wireless Communications and Networking*, Vol. 2023, No. 1, 27, Mar. 2023.

[23] Karad, K. V. and V. S. Hendre, "a foam-based compact flexible wideband antenna for healthcare applications," *Progress In Electromagnetics Research C*, Vol. 123, 197–212, 2022.

[24] Fernandez, M., H. G. Espinosa, D. V. Thiel, and A. Arrinda, "Wearable slot antenna at 2.45 GHz for off-body radiation: Analysis of efficiency, frequency shift, and body absorption," *Bioelectromagnetics*, Vol. 39, No. 1, 25–34, 2018.

[25] Fernandez, M., H. G. Espinosa, D. Guerra, I. Peña, D. V. Thiel, and A. Arrinda, "RF energy absorption in human bodies due to wearable antennas in the 2.4 GHz frequency band," *Bioelectromagnetics*, Vol. 41, No. 1, 73–79, 2020.